crystals

MDPI

Article

Where Are the tpy Embraces in $[Zn\{4'\text{-}(EtO)_2OPC_6H_4tpy\}_2][CF_3SO_3]_2$?

Davood Zare, Alessandro Prescimone, Edwin C. Constable and Catherine E. Housecroft *

Department of Chemistry, University Basel, BPR 1096, Mattenstrasse 24a, CH-4058 Basel, Switzerland; Davood.Zare@unibas.ch (D.Z.); alessandro.prescimone@unibas.ch (A.P.); Edwin.constable@unibas.ch (E.C.C.)

* Correspondence: catherine.housecroft@unibas.ch; Tel.: +41-61-207-1008

Received: 28 November 2018; Accepted: 7 December 2018; Published: 10 December 2018

Abstract: In this paper, the bromo- and phosphonate-ester-functionalized complexes $[Zn(\mathbf{1})_2][CF_3SO_3]_2$ and $[Zn(\mathbf{2})_2][CF_3SO_3]_2$ (**1** = 4′-(4-bromophenyl)-2,2′:6′,2″-terpyridine, **2** = diethyl (4-([2,2′:6′,2″-terpyridin]-4′-yl)phenyl)phosphonate) are reported. The complexes have been characterized by electrospray mass spectrometry, IR and absorption spectroscopies, and multinuclear NMR spectroscopy. The single-crystal structures of $[Zn(\mathbf{1})_2][CF_3SO_3]_2{\cdot}MeCN{\cdot}{}^1/_2Et_2O$ and $[Zn(\mathbf{2})_2][CF_3SO_3]_2$ have been determined and they confirm $\{Zn(tpy)_2\}^{2+}$ cores (tpy = 2,2′:6′,2″-terpyridine). Ongoing from X = Br to $P(O)(OEt)_2$, the $\{Zn(4'\text{-}XC_6H_4tpy)_2\}^{2+}$ unit exhibits significant "bowing" of the backbone, which is associated with changes in packing interactions. The $[Zn(\mathbf{1})_2]^{2+}$ cations engage in head-to-tail 4′-Phtpy...4′-Phtpy embraces with efficient pyridine...phenylene π-stacking interactions. The $[Zn(\mathbf{2})_2]^{2+}$ cations pack with one of the two ligands involved in pyridine...pyridine π-stacking; steric hindrance between one $C_6H_4PO(OEt)_2$ group and an adjacent pair of π-stacked pyridine rings results in distortion of backbone of the ligand. This report is the first crystallographic determination of a salt of a homoleptic $[M\{4'\text{-}(RO)_2OPC_6H_4tpy\}_2]^{n+}$ cation.

Keywords: phosphonate ester; zinc(II); 2,2′:6′,2″-terpyridine; crystal structure

1. Introduction

The oligopyridines are archetypal metal-binding domains used as scaffolds for numerous functional architectures [1–3]. 2,2′:6′,2″-Terpyridines (tpy) are of particular interest as they are particularly readily accessible through simple synthetic procedures [4], and improvements to synthetic procedures continue to be reported [5]. Furthermore, implementations of oligopyridine ligands to novel target technologies continue to emerge, including optoelectronic devices [6,7]. Dye-sensitized solar cells (DSCs) utilize metal complexes as sensitizers for semiconductors [8] and the vast majority incorporate oligopyridine ligands [9]. The binding of the complex to the surface is through an anchoring ligand [10], which is typically an oligopyridine bearing carboxylic acid groups. Phosphonic acid anchoring groups have been shown to bind more strongly to semiconductor oxide surfaces than carboxylic acids and we have been particularly interested in the use of the phosphonic acid anchoring ligands shown in Scheme 1. The phosphonic acid anchor has been shown to be effective in complexes containing $\{Ru(bpy)_2(C\text{^}N)\}^+$ [11,12], $\{Cu(bpy)_2\}^+$ [13,14], and $\{Zn(tpy)_2\}^+$ [15,16] cores (C^N = a cyclometallating ligand such as the conjugate base of 2-phenylpyridine, bpy = 2,2′-bipyridine,), and we have demonstrated that, in copper-based dyes, the presence of both a 1,4-phenylene spacer between a bpy metal-binding domain and the phosphonic acid is beneficial to DSC performance [17]. The tpy derivative shown in Scheme 1 has been used in a number of $\{Ru(tpy)_2\}^+$- and $\{Zn(tpy)_2\}^+$-based dyes [15–22], and theoretical studies indicate that the

presence of the 1,4-phenylene spacer enhances the rate of electron-transfer across the dye/semiconductor interface [23].

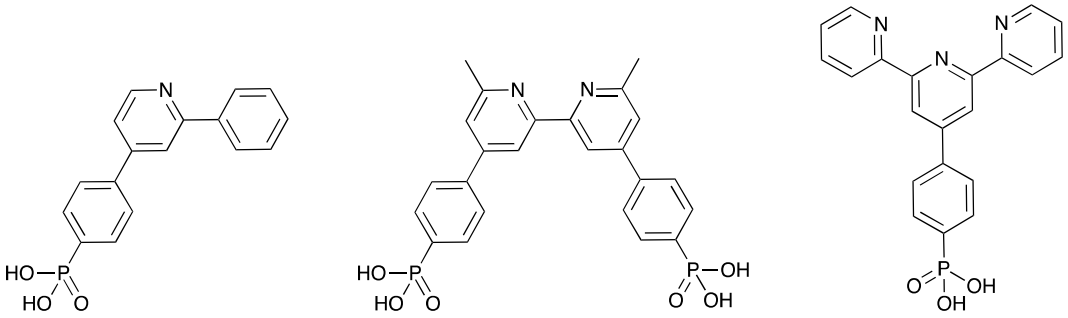

Scheme 1. Examples of anchoring ligands (cyclometallating H(C^N), bpy N^N, and tpy N^N^N) used in sensitizers in metal complex dyes in dye-sensitized solar cells.

Despite the interest in sensitizers based on polypyridine metal complexes incorporating phosphonic acid anchors, there is remarkably little crystallographic data available to provide insights into structural details, in particular, packing interactions that may influence aggregation of the surface-adsorbed species. A search of the CSD (v. 5.40, November 2018 [24] for metal-bonded {4′-O_3P-tpy} or {4′-O_3P-C_6H_4tpy} units gave surprisingly few hits [25–32], with only one featuring a 1,4-phenylene spacer [32]. It is also interesting to note that all of the reported structures relate to phosphonate esters rather than the parent phosphonic acids, and that the majority of the studies were motivated by application of the complexes as logic gates, photosensitizers, and catalysts. Here, we report the syntheses and single-crystal structures of the two zinc(II) complexes [Zn(**1**)$_2$][CF_3SO_3]$_2$ and [Zn(**2**)$_2$][CF_3SO_3]$_2$ (where ligands **1** and **2** are defined in Scheme 2) and investigate the effects that the phosphonate ester group has on intermolecular interactions in the solid state.

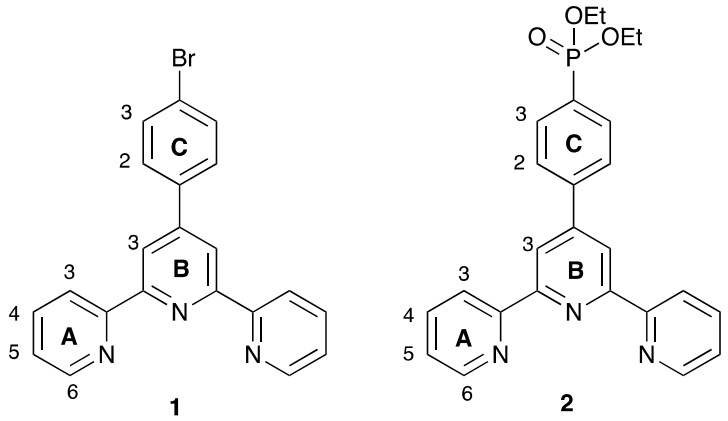

Scheme 2. Structures of the ligands **1** and **2**.

2. Materials and Methods

2.1. General

^{1}H, ^{13}C, and ^{31}P NMR spectra were recorded on a Bruker Avance III-500 spectrometer (Bruker BioSpin AG, Fällanden, Switzerland) at 298 K. The ^{1}H and ^{13}C NMR chemical shifts were referenced with respect to residual solvent peaks (δ TMS = 0), and ^{31}P shift with respect to 85% aqueous H_3PO_4. A Shimadzu LCMS-2020 instrument (Shimadzu Schweiz GmbH, Roemerstr., Switzerland) was used to record electrospray ionization (ESI) mass spectra. Solution absorption spectra were measured using a Cary 5000 spectrophotometer (Agilent, Lautengartenstr. 6, Basel, Switzerland). Solid-state IR

spectra were recorded using a Perkin Elmer UATR Two spectrometer (Perkin Elmer, Bahnstrasse 8, Schwerzenbach, Switzerland).

Compound **1** was prepared by the one-pot method of Wang and Hanan [33], and compound **2** was prepared from **1** by the method reported in [34].

2.2. $[Zn(1)_2][CF_3SO_3]_2$

A solution of $Zn(CF_3SO_3)_2$ (155 mg, 0.426 mmol) in MeCN (10 mL) was added to a solution of the **1** (347 mg, 0.895 mmol) in MeCN (10 mL). The reaction mixture was heated at 55 °C for 15 h and then the product was precipitated from the colourless solution by the addition of Et_2O. The precipitate was collected by filtration, washed with cold CH_2Cl_2 and Et_2O, and dried under vacuum. $[Zn(\mathbf{1})_2][CF_3SO_3]_2$ was isolated as a white microcrystalline solid (437 mg, 0.383 mmol, 89.9%). Slow diffusion of Et_2O into a solution of the complex in MeCN gave colourless single crystals suitable for X-ray crystallography. ^{1}H NMR (CD_3CN, 500 MHz) δ/ppm: 8.98 (s, 4H, H^{B3}), 8.72 (dt, J = 8.1, 1.0 Hz, 4H, H^{A3}), 8.43 (td, J = 7.8, 1.6 Hz, 4H, H^{A4}), 8.13 (m, 4H, H^{C2}), 7.95 (m, 4H, H^{C3}), 7.88 (m, 4H, H^{A6}), 7.42 (m, 4H, H^{A5}). ^{13}C NMR (CD_3CN, 126 MHz) δ/ppm: 156.1 (C^{B4}), 150.9 ($C^{A2/B2}$), 149.0 (C^{A6}), 148.8 ($C^{A2/B2}$), 142.2 (C^{A4}), 136.3 (C^{C1}), 133.7 (C^{C3}), 130.9 (C^{C2}), 128.5 (C^{A5}), 126.3 (C^{C4}), 124.2 (C^{A3}), 122.5 (C^{B3}). ESI-MS (MeOH, positive mode): m/z 990.90 $[M - CF_3SO_3]^+$ (calcd. 990.95), 421.60 $[M - 2CF_3SO_3]^{2+}$ (calcd. 421.00). UV-VIS (CH_3CN, 2.25 × 10^{-4} mol·dm^{-3}) λ_{max} (ε) 235 (25700). 256 (sh, 20900), 282 (sh, 32300), 289 (35300), 311 (sh, 25600), 329 (20700), 341 nm (16,800 dm^3·mol^{-1}·cm^{-1}). IR (see Figure S1). $C_{44}H_{28}Br_2F_6N_6O_6S_2Zn$ requires C 46.36, H 2.48, N 7.37; found C 45.57, H 3.17, N 7.30%.

2.3. $[Zn(2)_2][CF_3SO_3]_2$

The method was as for $[Zn(\mathbf{1})_2][CF_3SO_3]_2$ but starting with $Zn(CF_3SO_3)_2$ (59.6 mg, 0.164 mmol) and **2** (445 mg, 0.337 mmol). $[Zn(\mathbf{2})_2][CF_3SO_3]_2$ was isolated as a white microcrystalline solid (190 mg, 0.152 mmol, 92.7%). X-ray quality crystals were grown by slow diffusion of Et_2O into an MeCN solution of $[Zn(\mathbf{2})_2][CF_3SO_3]_2$. ^{1}H NMR ($CD_3CN$, 500 MHz) δ/ppm: 9.00 (s, 4H, H^{B3}), 8.72 (dt, J = 8.1, 1.0 Hz, 4H, H^{A3}), 8.29 (m, 4H, H^{C2}), 8.18 (td, J = 7.8, 1.6 Hz, 4H, H^{A4}), 8.12 (m, 4H, H^{C3}), 7.84 (ddd, J = 5.1, 1.7, 0.9 Hz, 4H, H^{A6}), 7.41 (m, 4H, H^{A5}), 4.19 (m, 8H, H^{Et}), 1.36 (t, J = 7.0 Hz, 12H, H^{Et}). ^{13}C NMR (CD_3CN, 126 MHz) δ/ppm: 156.3 (C^{B4}), 151.0 (C^{B2}), 149.1 (C^{A6}), 148.7 (C^{A2}), 142.3 (C^{A4}), 140.9 (C^{C1}), 133.5 (d, J_{PC} = 9.9 Hz, C^{C3}), 132.0 (C^{C4}), 129.3 (d, J_{PC} = 14.9 Hz, C^{C2}), 128.6 (C^{A5}), 124 3 (C^{A3}), 123.0 (C^{B3}), 63.3 (d, J_{PC} = 5.6 Hz, C^{Et}), 16.7 (d, J_{PC} = 6.2 Hz, C^{Et}). ^{31}P{^{1}H} NMR (CD_3CN, 202 MHz) δ/ppm +16.3 (s). ESI-MS (MeOH, positive mode): m/z 1103.20 $[M - CF_3SO_3]^+$ (calcd. 1103.19), 477.65 $[M - 2CF_3SO_3]^{2+}$ (calcd. 477.12). UV-VIS (CH_3CN, 1.55 × 10^{-4} mol·dm^{-3}) λ_{max} (ε) 234 (23900), 266 (sh, 29100), 281 (sh, 43000), 288 (47500), 324 (15800), 342 nm (16,000 dm^3·mol^{-1}·cm^{-1}). IR (see Figure S2). $C_{52}H_{48}F_6N_6O_{12}P_2S_2Zn$ requires C 49.79, H 3.86, N 6.70; found C 48.96, H 4.05, N 6.80%.

2.4. Crystallography

Single-crystal data were collected on a Bruker APEX-II diffractometer (Bruker AXS GmbH, Karlsruhe, Germany); data reduction, solution, and refinement used APEX2, SuperFlip, and CRYSTALS, respectively [35–37]. Structure analysis used Mercury v. 3.6 [38,39].

$[Zn(\mathbf{1})_2][CF_3SO_3]_2$·MeCN·1/2$Et_2O$: $C_{48}H_{36}Br_2F_6N_7O_{6.5}S_2Zn$, M = 1218.17, colourless block, triclinic, space group P–1, a = 12.1814(12), b = 14.7510(15), c = 15.1416(15) Å, α = 79.980(3), β = 69.658(3), γ = 71.317(3)°, U = 2410.6(4) Å^3, Z = 2, D_c = 1.678 Mg m^{-3}, μ(Cu-Kα) = 4.177 mm^{-1}, T = 123 K. Total 26609 reflections, 8560 unique, R_{int} = 0.029. Refinement of 8388 reflections (647 parameters) with $I > 2\delta(I)$ converged at final $R1$ = 0.0411 ($R1$ all data = 0.0416), $wR2$ = 0.0939 ($wR2$ all data = 0.0940), gof = 0.9775. CCDC 1879484.

$[Zn(\mathbf{2})_2][CF_3SO_3]_2$: $C_{52}H_{48}F_6N_6O_{12}P_2S_2Zn$, M = 1254.43, colourless block, monoclinic, space group $P2_1/n$, a = 15.7260(10), b = 15.6566(10), c = 22.9286(15) Å, β = 106.899(2)°, U = 5401.6(6) Å^3, Z = 4, D_c = 1.542 Mg m^{-3}, μ(Cu-Kα) = 2.693 mm^{-1}, T = 123 K. Total 69834 reflections, 9917 unique, R_{int} = 0.033. Refinement of 9379 reflections (730 parameters) with $I > 2\ \delta(I)$ converged at final $R1$ = 0.0372 ($R1$ all data = 0.0388), $wR2$ = 0.0923 ($wR2$ all data = 0.0924), gof = 1.0280. CCDC 1879482.

3. Results and Discussion

3.1. Synthesis and Solution Characterization of Complexes

Ligands **1** and **2** were prepared as previously reported [33,34]. Reaction of zinc(II) triflate with two equivalents of **1** or **2** resulted in the formation of $[Zn(\mathbf{1})_2][CF_3SO_3]_2$ and $[Zn(\mathbf{2})_2][CF_3SO_3]_2$ in 89.9% and 92.7% yield after purification. The electrospray mass spectra of the compounds showed peak envelopes with *m*/*z* 990.90 and 1103.20, respectively, arising from the $[M - CF_3SO_3]^+$ ion; the observed isotope distribution matched the simulation (Figures S3 and S4). The base peak in each spectrum corresponded to the $[M - 2CF_3SO_3]^{2+}$ ion with half-mass separations between the peaks in the peak-envelope. The ^1H and ^{13}C NMR spectra were assigned by 2D methods. Figures 1 and 2 display the aromatic regions of the ^1H NMR spectra, with the full spectra shown in Figures S5 and S6. COSY and HMQC spectra are shown in Figures S7–S10. The shift to lower frequency for the proton H^{A6} (see Scheme 2 for labelling) ongoing from free to coordinated ligand was typical of the formation of the {M(tpy)$_2$} unit, with H^{A6} lying over the π-system of the adjacent ligand. For example, in **2** (in $CDCl_3$), the resonance for H^{A6} appeared at δ 8.74 ppm [34], while in $[Zn(\mathbf{2})_2][CF_3SO_3]_2$ (in CD_3CN), it was at δ 7.88 ppm. In $[Zn(\mathbf{1})_2][CF_3SO_3]_2$, the ^1H NMR signal for H^{C2} showed a NOESY cross-peak to the signal for H^{B3} (Figure S11). Assignment in $[Zn(\mathbf{2})_2][CF_3SO_3]_2$ was also aided by characteristic coupling between the ^{31}P nucleus and protons H^{C2} and H^{C3}, respectively (Figure 2). $[Zn(\mathbf{2})_2][CF_3SO_3]_2$ exhibited a signal at δ +16.3 ppm in its ^{31}P NMR spectrum. The ethoxy groups in $[Zn(\mathbf{2})_2][CF_3SO_3]_2$ were characterized by multiplets at δ 4.19 and 1.36 ppm in the ^1H NMR spectrum and by doublets at δ 63.3 ppm (J_{PC} = 5.6 Hz) and δ 16.7 ppm (J_{PC} = 6.2 Hz. The IR spectra of $[Zn(\mathbf{1})_2][CF_3SO_3]_2$ and $[Zn(\mathbf{2})_2][CF_3SO_3]_2$ are shown in Figures S1 and S2. The most significant difference was an absorption at 959 cm^{-1} assigned to ν(P–O) in $[Zn(\mathbf{2})_2][CF_3SO_3]_2$.

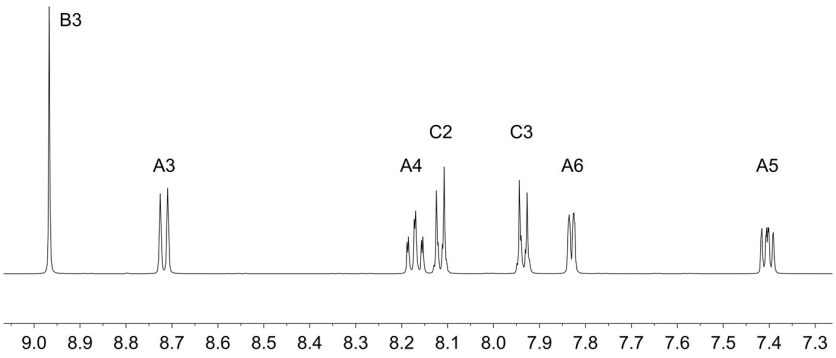

Figure 1. The ^1H NMR spectrum (500 MHz, CD_3CN) of $[Zn(\mathbf{1})_2][CF_3SO_3]_2$ (see also Figure S5). See Scheme 2 for atom labels.

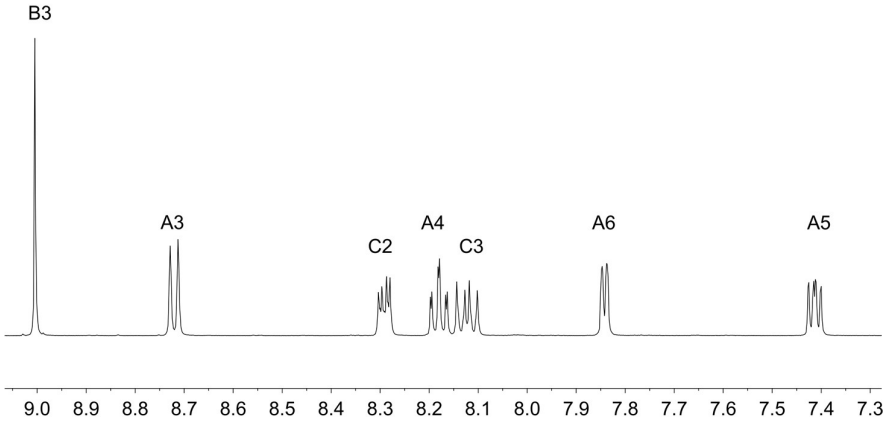

Figure 2. The ^1H NMR spectrum (500 MHz, CD_3CN) of $[Zn(\mathbf{2})_2][CF_3SO_3]_2$ (see also Figure S6). See Scheme 2 for atom labels.

3.2. Crystal Structures of [Zn(1)$_2$][CF$_3$SO$_3$]$_2$·MeCN·$^1/_2$Et$_2$O and [Zn(2)$_2$][CF$_3$SO$_3$]$_2$

Colourless single crystals of [Zn(**1**)$_2$][CF$_3$SO$_3$]$_2$·MeCN·$^1/_2$Et$_2$O and [Zn(**2**)$_2$][CF$_3$SO$_3$]$_2$ were grown by diffusion of Et$_2$O into MeCN solutions of the compounds. The two compounds crystallized in the triclinic *P*–1 and monoclinic *P*2$_1$/*n* space groups, respectively. Despite there being a wide range of crystallographically determined salts of [Zn(4′-Rtpy)$_2$]$^{2+}$ (4′-Rtpy is a 4′-functionalized tpy), we were surprised to find no salts of [Zn(**1**)$_2$]$^{2+}$ in the CSD (v. 5.39 with updates [24]. Figures 3 and 4 display the structures of the [Zn(**1**)$_2$]$^{2+}$ and [Zn(**2**)$_2$]$^{2+}$ cations, with selected bond distances and angles given in the captions to the figures. The Zn–N bond lengths were typical of {Zn(tpy)$_2$}$^{2+}$ units, as were the N–Zn–N chelate angles. On going from the bromo to diethylphosphonate derivative, the tpy units become ruffled. In [Zn(**1**)$_2$]$^{2+}$, the angles between the planes of adjacent pyridine rings in the two ligands were 12.7° and 3.5°, and 9.7° and 2.6°. In contrast, in [Zn(**2**)$_2$]$^{2+}$, the corresponding angles were 8.0° and 19.0°, and 11.3° and 20.6°. Differences in the twist of the C$_6$H$_4$ ring with respect to the central pyridine of the tpy unit (21.0° and 32.3° for the two ligands in [Zn(**1**)$_2$]$^{2+}$, and 30.6° and 34.0° in [Zn(**2**)$_2$]$^{2+}$) were rationalized in terms of the different molecular packings discussed below.

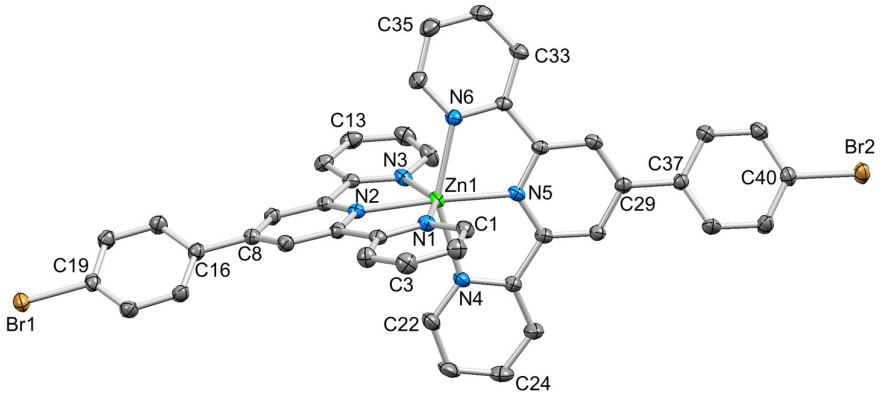

Figure 3. ORTEP-style depiction of the [Zn(**1**)$_2$]$^{2+}$ cation. Hydrogen atoms omitted and ellipsoids plotted at 50% probability level. Selected bond parameters: Zn1–N1 = 2.179(2), Zn1–N2 = 2.087(2), Zn1–N3 = 2.198(2), Zn1–N4 = 2.212(2), Zn1–N5 = 2.079(2), Zn1–N6 = 2.169(2), C19–Br1 = 1.896(3), C40–Br2 = 1.900(3) Å; N2–Zn1–N5 = 174.89(9)°, N6–Zn1–N4 = 150.79(9)°, N2–Zn1–N1 = 75.46(9)°, N2–Zn1–N3 = 74.87(9)°, N5–Zn1–N4 = 75.22(9)°, N6–Zn1–N5 = 75.65(9)°.

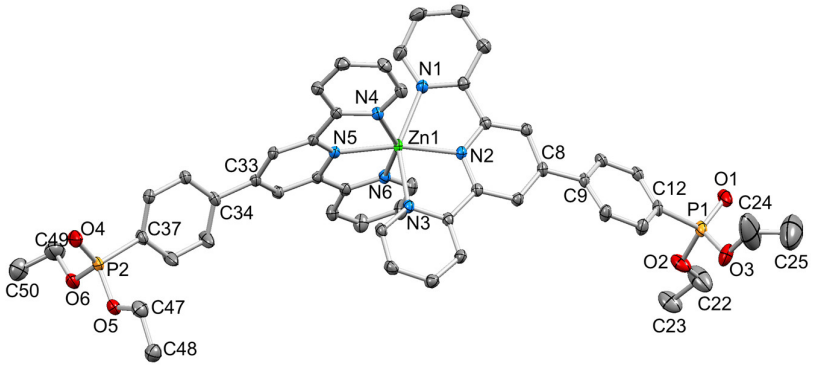

Figure 4. ORTEP-style diagram of the [Zn(**2**)$_2$]$^{2+}$ cation. Ellipsoids plotted at 50% probability level; H atoms omitted. Selected bond parameters: Zn1–N1 = 2.2139(16), Zn1–N2 = 2.0760(14), Zn1–N3 = 2.2310(15), Zn1–N4 = 2.1701(15), Zn1–N5 = 2.0793(14), Zn1–N6 = 2.2157(15), P1–O1 = 1.4686(15), P1–O2 = 1.5713(15), P1–O3 = 1.5788(16), P2–O4 = 1.4683(15), P2–O5 = 1.5747(14), P2–O6 = 1.5829(16) Å; N2–Zn1–N5 = 167.72(6)°, N6–Zn1–N4 = 150.52(6)°, N2–Zn1–N1 = 75.28(5)°, N2–Zn1–N3 = 75.06(5)°, N5–Zn1–N4 = 76.23(6)°, N–Zn1–N6 = 74.75(6)°, O1–P1–O2 = 115.15(9)°, O1–P1–O3 = 115.54(9)°, O2–P1–O3 = 101.88(9)°, C12–P1–O1 = 114.01(9)°, C12–P1–O2 = 102.13(8)°, C12–P1–O3 = 106.55(9)°.

The packing of $[Zn(\mathbf{1})_2]^{2+}$ cations in $[Zn(\mathbf{1})_2][CF_3SO_3]_2{\cdot}MeCN{\cdot}^1/_2Et_2O$ involved one of the characteristic 4′-Phtpy...4′-Phtpy (4′-Phtpy = 4′-phenyl-2,2′:6′,2″-terpyridine) embraces described by McMurtrie and Dance [40,41]. This is shown in Figure 5, with the embrace involving ligands containing Br2 and N6^{i} (and N6 and Br2^{i}, symmetry code i = $-x$, 3 − y, 1 − z). The phenyl$_{centroid}$...pyridine$_{centroid}$ separation was 3.73 Å and the angle between the π-stacked ring planes was 8.5°. For the ligand with Br2, the twist of the C_6H_4 ring with respect to the central pyridine of the tpy unit (21.0°) was smaller than for the ligand with Br1 (32.3°); this difference is associated with the π-stacking shown in Figure 5. By symmetry (in the *P*–1 space group), the ligand containing Br1 is also involved in a head-to-tail packing interaction with an adjacent ligand (Figure 5), but in this case, the relative positions of the symmetry-related ligands did not allow for an effective embrace [40,41]. Interestingly, there were no short Br...Br contacts, as have been observed for $[Fe(\mathbf{1})_2][PF_6]_2$ and related complexes [42]. We note that atom Br1 lies 4.13 Å from the centroid of the pyridine ring containing N4ii (symmetry code *ii* = 2 − x, 2 − y, −z) but at the upper limit of a weak Br...π contact [43]. The triflate ions are involved in F...H–C and O...H–C interactions. However, without crystallographic data for other salts, it was not possible to assess how the counterion affects the packing of the $[Zn(\mathbf{1})_2]^{2+}$ cations.

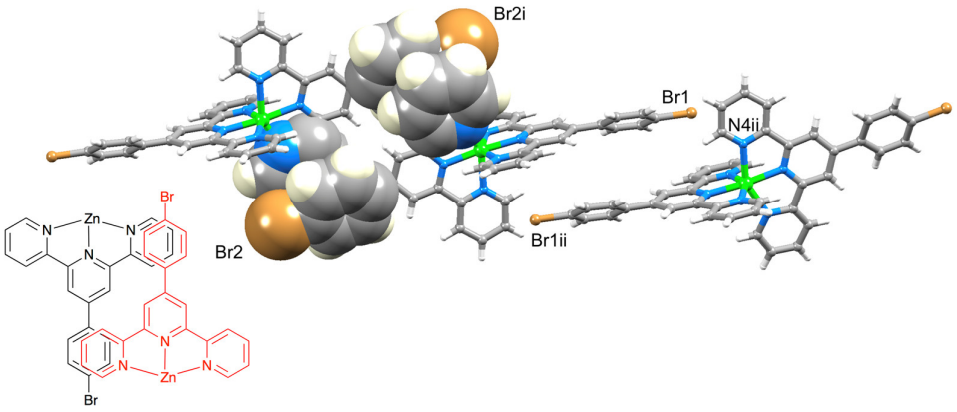

Figure 5. Packing interactions between centrosymmetric pairs of $[Zn(\mathbf{1})_2]^{2+}$ cations, and schematic representation of the 4′-Phtpy...4′-Phtpy embrace [37,38]. See text for symmetry codes.

A comparison of Figures 3 and 4 shows that going from bromo to phosphonate ester functionalities results in a significant "bowing" of the backbone of the $\{Zn(4'\text{-}XC_6H_4tpy)_2\}^{2+}$ unit, as is emphasized in the overlay in Figure 6. We have previously noted this feature in a number of compounds containing central $\{M(4'\text{-}XC_6H_4tpy)\}^{2+}$ motifs. However, detailed analysis of the packing interactions did not reveal a universal explanation for the phenomenon [44–46]. The bowing of the backbone in $[Zn(\mathbf{2})_2]^{2+}$ could be quantified by the C19...Zn1...C40 angle of 168.5° in $[Zn(\mathbf{1})_2]^{2+}$ (Figure 3) vs. the C12...Zn1...C37 (Figure 4) angle of 145.2° in $[Zn(\mathbf{2})_2]^{2+}$. $[Zn(\mathbf{2})_2][CF_3SO_3]_2$ crystallized without solvent in the lattice and solvent effects can be excluded as the cause of the deviation from an ideal C12...C37 vector in $[Zn(\mathbf{2})_2]^{2+}$. Important cation...cation contacts are illustrated in Figure 7. Pyridine rings containing N4 and N4^{i} engage in the face-to-face π-stacking interaction shown in Figure 7a with centroid...centroid and interplane separations of 3.63 and 3.24 Å, respectively. Symmetry-related intercation π-stacking contacts result in the formation of double-chains of cations running parallel to the crystallographic *b*-axis (Figure 7a). The bending of the backbone of the ligand incorporating atoms P1 and O1 appears to be associated with steric hindrance between the $C_6H_4PO(OEt)_2$ group and an adjacent pair of π-stacked pyridine rings. This also leads to close P–O...H–C contacts as shown in Figure 7b, parameters for which are O1...H271^{ii} = 2.43 Å, O1...H211^{iii} = 2.58 Å, and O1...H201^{iii} = 2.69 Å (symmetry codes are defined in the caption to Figure 7). Chains are further associated through short P–O...H–C contacts between phosphate ester groups of adjacent cations (Figure 8). This involves atom O5 (attached to P2) and H222^{iv} of the OCH_2 group attached to P1^{iv} (Figure 8b). Comparisons of the packing interactions in $[Zn(\mathbf{2})_2][CF_3SO_3]_2$ with related structures

are limited by the lack of structural information (see Section 1: Introduction). However, analysis of the structure of [ReCl{4′(4-$(MeO)_2OPC_6H_4$tpy}$_2$] (which contains a 7-coordinate Re(III) centre) revealed that the dominant features in the packing involved close OMe...π_{arene} contacts rather than tpy...tpy π-stacking (CSD refcode PACXOI) [32].

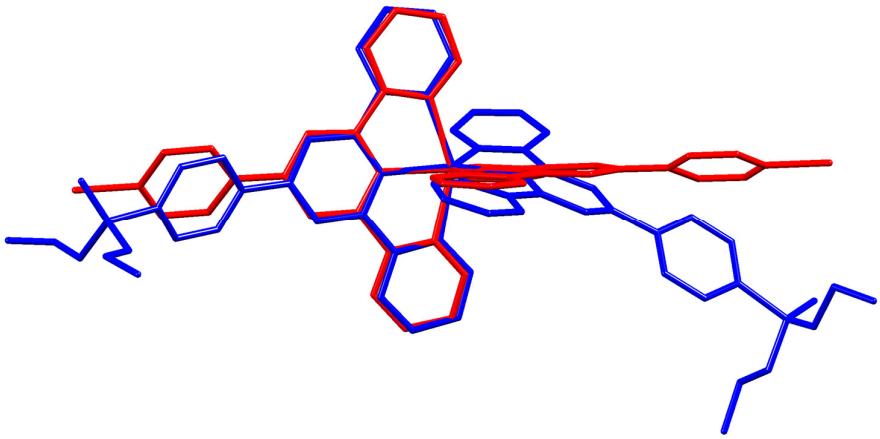

Figure 6. Overlay of the structures of the $[Zn(\mathbf{1})_2]^{2+}$ (red) and $[Zn(\mathbf{2})_2]^{2+}$ (blue) cations (H atoms omitted). Pairs of atoms Zn1, N2, N5, and N1 were superimposed to within ±0.13 Å.

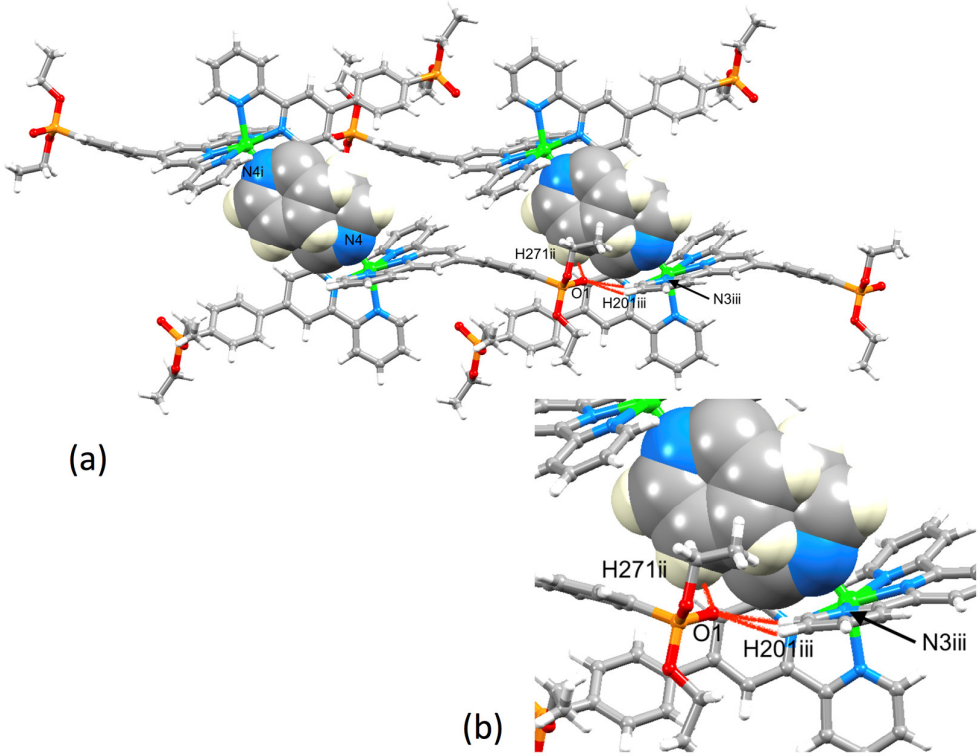

Figure 7. (**a**) Intercation packing interactions between $[Zn(\mathbf{2})_2]^{2+}$ cations in $[Zn(\mathbf{2})_2][CF_3SO_3]_2$ and (**b**) expansion of the close P–O...H–C contacts. Anions are omitted. Symmetry codes: *i* = −*x*, 1 − *y*, 1 − *z*; *ii* = −*x*, −*y*, 1 − *z*; *iii* = *x*, −1+*y*, +*z*.

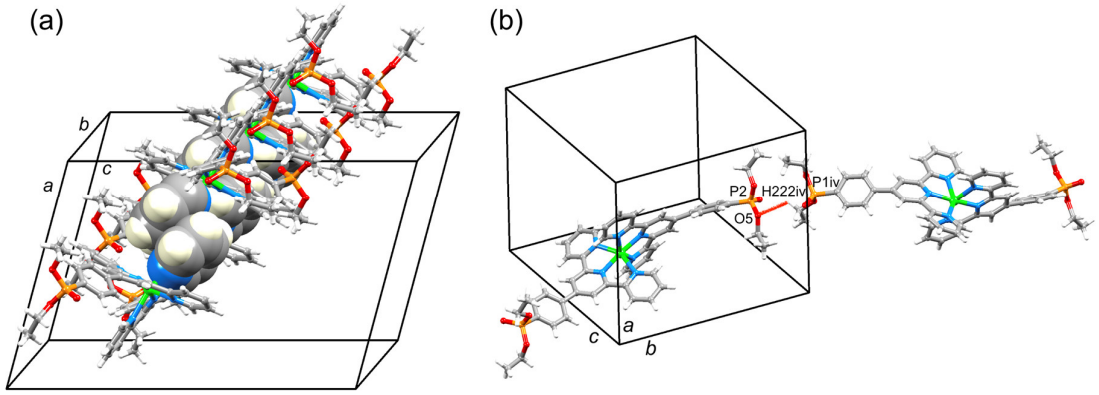

Figure 8. (**a**) Part of one chain of $[Zn(\mathbf{2})_2]^{2+}$ cations in $[Zn(\mathbf{2})_2][CF_3SO_3]_2$ supported by pyridine...pyridine π-stacking interactions. (**b**) Short PO...HC contact between phosphate ester groups of adjacent cations. Symmetry code iv = $^1/_2-x$, $^3/_2+y$, $^1/_2-z$.

4. Conclusions

We have prepared the bromo- and phosphonate-ester-functionalized bis(tpy) complexes $[Zn(\mathbf{1})_2][CF_3SO_3]_2$ and $[Zn(\mathbf{2})_2][CF_3SO_3]_2$, and electrospray mass spectrometric and multinuclear NMR spectroscopic data were consistent with the formation of the homoleptic complexes. The single-crystal structures of $[Zn(\mathbf{1})_2][CF_3SO_3]_2{\cdot}MeCN{\cdot}^1/_2Et_2O$ and $[Zn(\mathbf{2})_2][CF_3SO_3]_2$ were determined and confirmed the expected octahedral coordination of the Zn^{2+} ion in each complex. Significant bowing of the backbone of the $\{Zn(4'\text{-}XC_6H_4tpy)_2\}^{2+}$ unit was observed ongoing from bromo to phosphonate ester functionalities and was associated with changes in packing interactions. The $[Zn(\mathbf{1})_2]^{2+}$ cations engaged in head-to-tail 4′-Phtpy...4′-Phtpy embraces with efficient pyridine...phenylene π-stacking interactions. In contrast, $[Zn(\mathbf{2})_2]^{2+}$ cations packed with one of the two ligands involved in pyridine...pyridine π-stacking; steric hindrance between one $C_6H_4PO(OEt)_2$ group and an adjacent pair of π-stacked pyridine rings resulted in distortion of the backbone of the ligand. Short P–O...H–C contacts between phosphate ester groups were also observed. This investigation was the first crystallographic determination of a salt of a homoleptic $[M\{4'\text{-}(RO)_2OPC_6H_4tpy\}_2]^{n+}$ cation.

Supplementary Materials: The following are available online at www.mdpi.com/xxx/s1. Figures S1 and S2: IR spectra of $[Zn(\mathbf{1})_2][CF_3SO_3]_2$ and $[Zn(\mathbf{2})_2][CF_3SO_3]_2$. Figures S3–S11: Additional NMR spectra of $[Zn(\mathbf{1})_2][CF_3SO_3]_2$ and $[Zn(\mathbf{2})_2][CF_3SO_3]_2$.

Author Contributions: D.Z.: Ligand and complex synthesis and characterization, consolidation of data; A.P.: Crystallography; E.C.C.: Group leader, project concepts, and contributions to manuscript preparation; C.E.H.: Group leader, project concepts, and manuscript preparation.

Funding: We thank the Swiss National Science Foundation and the University of Basel for support.

Conflicts of Interest: The authors declare no conflict of interest.

References

1. Constable, E.C. Homoleptic complexes of 2,2′-bipyridine. *Adv. Inorg. Chem.* **1989**, *34*, 1–63. doi:10.1016/S0898-8838(08)60014-8.
2. Constable, E.C. The coordination chemistry of 2,2′:6′,2″-terpyridine and higher oligopyridines. *Adv. Inorg. Chem. Radiochem.* **1986**, *30*, 69–121. doi:10.1016/S0898-8838(08)60240-8.
3. Constable, E.C. 2,2′:6′,2″-Terpyridines: From chemical obscurity to common supramolecular motifs. *Chem. Soc. Rev.* **2007**, *36*, 246–253. doi:10.1039/B601166G.
4. Schubert, U.S.; Hofmeier, H.; Newkome, G.R. *Modern Terpyridine Chemistry*; Wiley-VCH: Weinheim, Germany, 2006; ISBN 978-3-527-31475-1.

5. Zamalyutin, V.V.; Bezdenezhnykh, V.A.; Nichugovskiy, A.I.; Flid, V.R. New approaches to the synthesis of 2,2′:6′,2″-terpyridine and some of its derivatives. *Russ. J. Org. Chem.* **2018**, *54*, 419–425. doi:10.1134/S1070428018030089.
6. Schubert, U.S.; Winter, A.; Newkome, G.R. *Terpyridine-Based Materials: For Catalyic, Optoelectronic and Life Sciene Applications*; Wiley-VCH: Weinheim, Germany, 2012; ISBN 978-3-527-33038-6.
7. Laschuk, N.O.; Ebralidze, I.I.; Poisson, J.; Egan, J.G.; Quaranta, S.; Allan, J.T.S.; Cusden, H.; Gaspari, F.; Naumkin, F.Y.; Easton, E.B.; et al. Ligand Impact on Monolayer Electrochromic Material Properties. *ACS Appl. Mater. Interfaces* **2018**, *10*, 35334–35343. doi:10.1021/acsami.8b10666.
8. Nazeeruddin, M.K.; Baranoff, E.; Grätzel, M. Dye-sensititzed solar cells: A brief review. *Sol. Energy* **2011**, *85*, 1172–1178. doi:10.1016/j.solener.2011.01.018.
9. Aghazada, S.; Nazeeruddin, M.K. Ruthenium complexes as sensitisers in dye-sensititzed solar cells. *Inorganics* **2018**, *6*, 52. doi:10.3390/inorganics6020052.
10. Zhang, L.; Cole, J.M. Anchoring groups for dye-sensitized solar cells. *ACS Appl. Mater. Interfaces* **2015**, *7*, 3427–3455. doi:10.1021/am507334m.
11. Marinakis, N.; Willgert, M.; Constable, E.C.; Housecroft. C.E. Optimization of performance and long-term stability of p-type dye-sensitized solar cells with a cycloruthenated dye through electrolyte solvent tuning. *Sustain. Energy Fuels* **2017**, *1*, 626–635. doi:10.1039/c7se00060j.
12. Marinakis, N.; Wobill, C.; Constable, E.C.; Housecroft, C.E. Refining the anchor: Optimizing the performance of cyclometallated ruthenium(II) dyes in p-type dye sensitized solar cells. *Polyhedron* **2018**, *140*, 122–128. doi:10.1016/j.poly.2017.12.015.
13. Housecroft, C.E.; Constable, E.C. The emergence of copper(I)-based dye sensitized solar cells. *Chem. Soc. Rev.* **2015**, *44*, 8386–8398. doi:10.1039/C5CS00215J.
14. Malzner, F.J.; Housecroft, C.E.; Constable, E.C. The versatile SALSAC approach to heteroleptic copper(I) dye assembly in dye-sensitized solar cells. *Inorganics* **2018**, *6*, 57. doi:10.3390/inorganics6020057.
15. Bozic-Weber, B.; Constable, E.C.; Hostettler, N.; Housecroft, C.E.; Schmitt, R.; Schönhofer, E. The d^{10} route to dye-sensitized solar cells: Step-wise assembly of zinc(II) photosensitizers on TiO_2 surfaces. *Chem. Commun.* **2012**, *48*, 5727–5729. doi:10.1039/c2cc31729j.
16. Hostettler, N.; Fürer, S.O.; Bozic-Weber, B.; Constable, E.C.; Housecroft, C.E. Alkyl chain-functionalized hole-transporting domains in zinc(II) dye-sensitized solar cells. *Dyes Pigments* **2015**, *116*, 124–130. doi:10.1016/j.dyepig.2015.01.008.
17. Bozic-Weber, B.; Brauchli, S.Y.; Constable, E.C.; Fürer, S.O.; Housecroft, C.E.; Malzner, F.J.; Wright, I.A.; Zampese, J.A. Improving the photoresponse of copper(I) dyes in dye-sensitized solar cells by tuning ancillary and anchoring ligand modules. *Dalton Trans*. **2013**, *42*, 12293–12308. doi:10.1039/C3DT51416A.
18. Stergiopoulos, T.; Arabatzis, I.M.; Kalbac, M.; Lukes, I.; Falaras, P. Incorporation of innovative compounds in nanostructured photoelectrochemical cells. *J. Mater. Process. Technol*. **2005**, *161*, 107–112. doi:10.1016/j.jmatprotec.2004.07.014.
19. Stergiopoulos, T.; Bernard, M.-C.; Hugot-Le Goff, A.; Falaras, P. Resonance micro-Raman spectrophotoelectrochemistry on nanocrystalline TiO2 thin film electrodes sensitized by Ru (II) complexes. *Coord. Chem. Rev.* **2004**, *248*, 1407–1420. doi:10.1016/j.ccr.2004.03.023.
20. Krebs, F.C.; Biancardo, M. Dye sensitized photovoltaic cells: Attaching conjugated polymers to zwitterionic ruthenium dyes. *Solar Energy Mater. Solar Cells* **2006**, *90*, 142–165. doi:10.1016/j.solmat.2005.02.006.
21. Jing, B.; Zhang, H.; Zhang, M.; Lu, Z.; Shen, T. Ruthenium(II) thiocyanate complexes containing 4′-(4-phosphonatophenyl)-2,2′:6′,2″-terpyridine: Synthesis, photophysics and photosensitization to nanocrystalline TiO_2 electrodes. *J. Mater. Chem.* **1998**, *8*, 2055–2060. doi:10.1039/A802489H.
22. Wolpher, H.; Sinha, S.; Pan, J.; Johansson, A.; Lundqvist, M.J.; Persson, P.; Lomoth, R.; Bergquist, J.; Sun, L.; Sundström, V.; et al. Synthesis and electron transfer studies of ruthenium–

terpyridine-based dyads attached to nanostructured TiO_2. *Inorg. Chem.* **2007**, *46*, 638–651. doi:10.1021/ic060858a.
23. Lundqvist, M.J.; Nilsig, M.; Lunell, S.; Åkermark, B.; Persson, P. Spacer and anchor effects on the electronic coupling in ruthenium-bis-terpyridine dye-sensitized TiO_2 nanocrystals studied by DFT. *J. Phys. Chem. B* **2006**, *110*, 20513–20525. doi:10.1021/jp064045j.
24. Groom, C.R.; Bruno, I.J.; Lightfoot, M.P.; Ward, S.C. The Cambridge Structural Database. *Acta Crystallogr. Sect. B* **2016**, *72*, 171–179.
25. Laschuk, N.O.; Ebralidze, I.I.; Spasyuk, D.; Zenkina, O.V. Multi-readout logic gate for the selective detection of metal ions at the parts per billion level. *Eur. J. Inorg. Chem.* **2016**, 3530–3535. doi:10.1002/ejic.201600606.
26. Constable, E.C.; Housecroft, C.E.; Neuburger, M.; Schneider, A.G.; Zehnder, M. The ditopic ligands 4′-(diphenylphosphino)-2,2′:6′,2″-terpyridine (**1**) and 4′-(oxodiphenylphosphanyl)-2,2′:6′,2″-terpyridine (**2**): Coordination to iron(II), ruthenium(II), cobalt(II) and palladium(II); X-ray crystal structures of $[Ru(\mathbf{2})_2][PF_6]_2{\cdot}MeCN{\cdot}H_2O$ and *trans*-$[Pd(\mathbf{1})_2Cl_2]{\cdot}2.5CH_2Cl_2$. *J. Chem. Soc. Dalton Trans.* **1997**, 2427–2434. doi:10.1039/A702023F.
27. Chen, W.; Rein, F.N.; Scott, B.L.; Rocha, R.C. (2,2′-Bipyridine)chlorido[diethyl(2,2′:6′,2″-terpyridin-4-yl)phosphonate]ruthenium(II) hexafluoridophosphate acetonitrile/water solvate. *Acta Crystallogr. Sect. E* **2013**, *69*, m510–m511. doi:10.1107/S1600536813022940.
28. Zakeeruddin, S.M.; Nazeeruddin, M.K.; Pechy, P.; Rotzinger, F.P.; Humphry-Baker, R.; Kalyanasundaram, K.; Grätzel, M.; Shklover, V.; Haibach, T. Molecular engineering of photosensitizers for nanocrystalline solar cells: Synthesis and characterization of Ru dyes based on phosphonated terpyridines. *Inorg. Chem*. **1997**, *36*, 5937–5946. doi:10.1021/ic970008i.
29. Francàs, L.; Richmond, C.; Garrido-Barros, P.; Planas, N.; Roeser, S.; Benet-Buchholz, J.; Escriche, L.; Sala, X.; Llobet, A. Ru–bis(pyridine)pyrazolate (bpp)-based water-oxidation catalysts anchored on TiO_2: The importance of the nature and position of the anchoring group. *Chem. Eur. J.* **2016**, *22*, 5261–5268. doi:10.1002/chem.201504015.
30. Ferrer, I.; Fontrodona, X.; Roig, A.; Rodríguez, M.; Romero, I. A recoverable ruthenium aqua complex supported on silica particles: An efficient epoxidation catalyst. *Chem. Eur. J.* **2017**, *23*, 4096–4107. doi:10.1002/chem.201604463.
31. Vaquer, L.; Riente, P.; Sala, X.; Jansat, S.; Benet-Buchholz, J.; Llobet, A.; Pericas, M.A. Molecular ruthenium complexes anchored on magnetic nanoparticles that act as powerful and magnetically recyclable stereospecific epoxidation catalysts. *Cat. Sci. Tech*. **2013**, *3*, 706–714. doi:10.1039/C2CY20616A.
32. Sugimoto, H.; Tano, H.; Miyake, H.; Itoh, S. Seven-coordinate rhenium(III) complexes with a labile coordination site assembled on indium-doped tin oxide (ITO) electrodes: Catalytic reduction of dioxygen to hydrogen peroxide. *Chem. Lett.* **2010**, *39*, 986–988. doi:10.1246/cl.2010.986.
33. Wang, J.; Hanan, G.S. A facile route to sterically hindered and non-hindered 4′-aryl-2,2′:6′,2″-terpyridines. *Synlett* **2005**, 1251–1254. doi:10.1055/s-2005-868481.
34. Spampinato, V.; Tuccitto, N.; Quici, S.; Calabrese, V.; Marletta, G.; Torrisi, A.; Licciardello, A. Functionalization of oxide surfaces by terpyridine phosphonate ligands: Surface reactions and anchoring geometry. *Langmuir* **2010**, *26*, 8400–8406. doi:10.1021/la9048314.
35. Bruker Analytical X-ray Systems. *APEX2, Version 2 User Manual*; M86-E01078; Bruker Analytical X-ray Systems, Inc.: Madison, WI, USA, 2006.
36. Palatinus, L.; Chapuis, G. SUPERFLIP—A computer program for the solution of crystal structures by charge flipping in arbitrary dimensions. *J. Appl. Cryst.* **2007**, *40*, 786–790. doi:10.1107/S0021889807029238.
37. Betteridge, P.W.; Carruthers, J.R.; Cooper, R.I.; Prout, K.; Watkin, D.J. CRYSTALS Version 12: Software for Guided Crystal Structure Analysis. *J. Appl. Cryst.* **2003**, *36*, 1487–1487. doi:10.1107/S0021889803021800.

38. Macrae, C.F.; Edgington, P.R.; McCabe, P.; Pidcock, E.; Shields, G.P.; Taylor, R.; Towler, M.; van de Streek, J. Mercury: Visualization and analysis of crystal structures. *J. Appl. Cryst.* **2006**, *39*, 453–457. doi:10.1107/S002188980600731X.
39. Macrae, C.F.; Bruno, I.J.; Chisholm, J.A.; Edgington, P.R.; McCabe, P.; Pidcock, E.; Rodriguez-Monge, L.; Taylor, R.; van de Streek, J.; Wood, P.A. Mercury CSD 2.0—New Features for the Visualization and Investigation of Crystal Structures. *J. Appl. Cryst*. **2008**, *41*, 466–470. doi:10.1107/S0021889807067908.
40. McMurtrie, J.; Dance, I. Crystal packing in metal complexes of 4′-phenylterpyridine and related ligands: Occurrence of the 2D and 1D terpy embrace arrays. *CrystEngComm* **2009**, *11*, 1141–1149. doi:10.1039/b821883h.
41. McMurtrie, J.; Dance, I. Alternative two-dimensional embrace nets formed by metal complexes of 4′-phenylterpyridine crystallised with hydrophilic anions. *CrystEngComm* **2010**, *12*, 3207–3217. doi:10.1039/c003035j.
42. Medleycott, E.A.; Hanan, G.S.; Abedin, T.S.M.; Thompson, L.K. The effect of steric hindrance on the Fe(II) complexes of triazine-containing ligands. *Polyhedron* **2008**, *27*, 493–501. doi:10.1016/j.poly.2007.10.002.
43. Shukla, R.; Panini, P.; McAdam, C.J.; Robinson, B.H.; Simpson, J.; Tagg, T.; Chopra, D. Characterization of non-classical C–Br...π interactions in (E)-1,3-dibromo-5-(2-(ferrocenyl)vinyl)benzene and related derivatives of ferocene. *J. Mol. Struct.* **2017**, *131*, 16–24. doi:10.1016/j.molstruc.2016.11.015.
44. Constable, E.C.; Housecroft, C.E.; Neuburger, M.; Schaffner, S.; Schaper, F. The solid-state structure of bis(4′-(4-pyridyl)-2,2′:6′,2″-terpyridine)ruthenium hexafluorophosphate nitrate—An expanded 4,4′-bipyridine. *Inorg. Chem. Commun.* **2006**, *9*, 616–619. doi:10.1016/j.inoche.2006.03.017.
45. Beves, J.E.; Constable, E.C.; Housecroft, C.E.; Kepert, C.J.; Neuburger, M.; Price, D.J.; Schaffner, S. The conjugate acid of bis{4′-(4-pyridyl)-2,2′:6′,2″-terpyridine}iron(II) as a self-complementary hydrogen-bonded building block. *CrystEngComm* **2007**, *9*, 1073–1077. doi:10.1039/b710332h.
46. Beves, J.E.; Bray, D.J.; Clegg, J.K.; Constable, E.C.; Housecroft, C.E.; Jolliffe, K.A.; Kepert, C.J.; Lindoy, L.F.; Neuburger, M.; Price, D.J.; et al. Expanding the 4,4′-bipyridine ligand: Structural variation in $\{M(pytpy)_2\}^{2+}$ complexes (pytpy = 4′-(4-pyridyl)-2,2′:6′,2″-terpyridine, M = Fe, Ni, Ru) and assembly of the hydrogen-bonded, one-dimensional polymer $\{[Ru(pytpy)(Hpytpy)]\}_n 3^{n+}$ *Inorg. Chim. Acta* **2008**, *361*, 2582–2590. doi:10.1016/j.ica.2007.10.040.